



Low carbon fuel production from combined solid oxide CO₂ co-electrolysis and Fischer-Tropsch synthesis system: A modelling study[☆]

Haoran Xu^a, M. Mercedes Maroto-Valer^{a,*}, Meng Ni^b, Jun Cao^c, Jin Xuan^{d,*}

^a Research Centre for Carbon Solutions (RCCS), School of Engineering & Physical Sciences, Heriot-Watt University, Edinburgh EH14 4AS, United Kingdom

^b Building Energy Research Group, Department of Building and Real Estate, The Hong Kong Polytechnic University, Hung Hom, Kowloon, Hong Kong, China

^c State Key Laboratory of Chemical Engineering, School of Mechanical and Power Engineering, East China University of Science and Technology, Shanghai, China

^d Department of Chemical Engineering, Loughborough University, Loughborough, United Kingdom

HIGHLIGHTS

- The first 2D combined CH₄-assisted SOEC and F-T synthesis model is developed.
- A novel strategy towards low-carbon fuel generation is proposed.
- Parametric studies are conducted with performance determining factors discussed.
- The distribution of generated carbon-contained fuels (from C₁ to C₅₊) is studied.

ARTICLE INFO

Keywords:

Solid oxide electrolyzer cell
Fischer-Tropsch synthesis
Mathematical modelling
Hydrocarbon generation

ABSTRACT

CH₄-assisted solid oxide electrolyzer cells (SOECs) can co-electrolyze H₂O and CO₂ effectively for simultaneous energy storage and CO₂ utilization. Compared with conventional SOECs, CH₄-assisted SOECs consume less electricity because CH₄ in the anode provides part of the energy for electrolysis. As syngas (CO and H₂ mixture) is generated from the co-electrolysis process, it is necessary to study its utilization through the subsequent processes, such as Fischer-Tropsch (F-T) synthesis to produce more value-added products. An F-T reactor can convert syngas into hydrocarbons, and thus it is very suitable for the utilization of syngas. In this paper, the combined CH₄-assisted SOEC and F-T synthesis system is numerically studied. Validated 2D models for CH₄-assisted SOEC and F-T processes are adopted for parametric studies. It is found that the cathode inlet H₂O/CO₂ ratio in the SOEC significantly affects the production components through the F-T process. Other operating parameters such as the operating temperature and applied voltage of the SOEC are found to greatly affect the productions of the system. This model is important for understanding and design optimization of the combined fuel-assisted SOEC and F-T synthesis system to achieve economical hydrocarbon generation.

1. Introduction

With the growing attention on global warming, effective CO₂ utilization methods are urgently needed [1]. Solid oxide electrolyzer cells (SOECs) are high-temperature technologies [2], which are suitable to convert CO₂ into chemicals or fuels by utilizing the renewable energy or excessive electricity produced from renewable resources [3]. SOECs are solid-state device working quietly at high efficiency [4]. In the SOEC, a dense ion-conducting electrolyte is sandwiched between two porous electrodes [5]. Compared with low-temperature electrolyzers, SOECs

consume less electrical energy as part of the input energy comes from heat [6]. The high operating temperature also allows the use of non-noble catalysts in the SOEC, leading to a lower overall cost [7]. In addition, solid oxide cells are suitable components to be combined in the hybrid systems such as the combination with Stirling cycle [8], the Otto heat engine [9] and the Vacuum thermionic generator [10] for overall performance improvement. Recently, the concept of fuel-assisted SOECs has been proposed and demonstrated [11], where low-cost fuels (e.g. methane from biogas or natural gas) are supplied to the anode to reduce the operating potentials of the SOEC. Through

[☆] The short version of the paper was presented at ICAE2018, Aug 22–25, Hong Kong. This paper is a substantial extension of the short version of the conference paper.

* Corresponding authors.

E-mail addresses: M.Maroto-Valer@hw.ac.uk (M.M. Maroto-Valer), j.xuan@lboro.ac.uk (J. Xuan).

<https://doi.org/10.1016/j.apenergy.2019.03.145>

Received 22 December 2018; Received in revised form 13 February 2019; Accepted 13 March 2019

Available online 21 March 2019

0306-2619/© 2019 The Authors. Published by Elsevier Ltd. This is an open access article under the CC BY license (<http://creativecommons.org/licenses/by/4.0/>).

Nomenclature			
Abbreviation		R_{MSR}	methane steam reforming reaction
F-T	Fischer Tropsch	R_{WGS}	water gas shift reaction
MSR	methane steam reforming	T	temperature, K
SCCM	standard cubic centime per minute	u	velocity field, $m^3 s^{-1}$
ScSZ	scandium stabilized zirconium	V	volume fraction
SOEC	solid oxide electrolyzer cell	y_i	mole fraction of component i
WGSR	water gas shift reforming	Greek letters	
YSZ	yttrium stabilized zirconium	α	charge transfer coefficient
Roman		β	activity factor, $A m^{-2}$
B_0	permeability coefficient, m^2	ε	porosity
D_i^{eff}	effective diffusivity of species i, $m^2 s^{-1}$	η_{act}	activation overpotential loss, V
D_{ik}^{eff}	Knudsen diffusion coefficient of i, $m^2 s^{-1}$	η_{ohmic}	Ohmic overpotential loss, V
D_{im}^{eff}	molecular diffusion coefficient of i, $m^2 s^{-1}$	κ	permeability, m^2
E_{act}	activation energy, $J mol^{-1}$	μ	dynamic viscosity of fluid, Pa s
E_{CO}	equilibrium potential for carbon monoxide oxidization, V	ρ	fluid density, $kg m^{-3}$
E_{CO}^0	standard equilibrium potential for carbon monoxide oxidization, V	σ	conductivity, S/m
E_{eq}	equilibrium Nernst potential, V	τ	tortuosity
E_{H_2}	equilibrium potential for hydrogen oxidization, V	Subscripts	
$E_{H_2}^0$	standard equilibrium potential for hydrogen oxidization, V	an	anode
F	Faraday constant, $96,485 C mol^{-1}$	ca	cathode
G	Gibbs free energy	CH ₄	methane
i	operating current density, $A m^{-2}$	CO	carbon monoxide
i_0	exchange current density, $A m^{-2}$	CO ₂	carbon dioxide
n	number of electrons transferred per electrochemical reaction	el	electrolyte
N_i	flux of mass transport, $kg m^{-3} s^{-1}$	H ₂	hydrogen
p	(partial) Pressure, Pa	H ₂ O	water
P_{CO}^L	local CO partial pressures, Pa	l	ionic phase
$P_{CO_2}^L$	local CO ₂ partial pressures, Pa	O ₂	oxygen
$P_{H_2}^L$	local H ₂ partial pressures, Pa	s	electronic phase
$P_{H_2O}^L$	local H ₂ O partial pressures, Pa	Superscripts	
$P_{O_2}^L$	local O ₂ partial pressures, Pa	0	parameter at equilibrium conditions
R	gas constant, $8.314 J mol^{-1} K^{-1}$	eff	effective
		L	local

experimental and numerical analysis [12], the CH₄-assisted SOEC has been demonstrated to have a higher electrochemical performance compared with the ones using CO as the assistant fuel. In some operating conditions, the fuel-assisted SOECs can even electrolyze oxidants without consuming electricity, which means it is possible to convert CO₂ to fuels by only consuming low-cost fuels in the SOEC [13]. Therefore, using SOECs for CO₂ recycle is an attractive solution for emission reduction [14].

SOECs can co-electrolyze H₂O and CO₂ and generate syngas (H₂ and

CO mixture) [15], which is a feedstock for the production of synthetic hydrocarbons via Fischer-Tropsch (F-T) process [16]. As methane is usually less wanted from the F-T process [17], it is therefore suitable to recycle methane from F-T reactor as the assistant fuel in the SOEC [18]. A system consisting of a CH₄-assisted SOEC and an F-T reactor can effectively convert CO₂ and generate desired hydrocarbons. Therefore, such a hybrid system is very promising for CO₂ utilization and hydrocarbon fuels generation. However, despite some preliminary studies on the combined SOEC and F-T systems through Techno-economic analysis

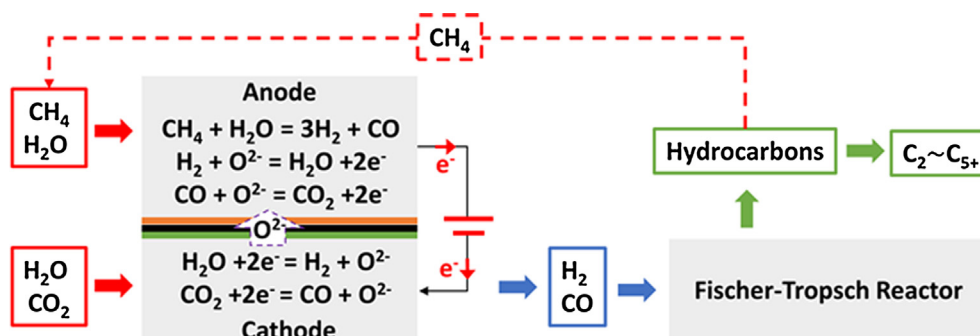


Fig. 1. Schematic of combined CH₄-assisted SOEC and F-T reactor system.

[19] and thermodynamic analysis [20], no detailed physicochemical, kinetics and thermofluids analysis on a combined fuel-assisted SOEC and F-T synthesis system has been conducted thus far.

To fill this research gap, in this work, 2D mathematical models are developed for a combined CH₄-assisted SOEC and F-T synthesis system for H₂O/CO₂ co-electrolysis and hydrocarbon fuels generation. The sub-models for the CH₄-assisted SOEC [21] and the F-T reactor [22] are validated in the previous studies. Parametric simulations are conducted to understand the characteristics of such a system and the interplay of different physical/chemical processes.

2. Model description

The proposed hybrid system consists of a CH₄-assisted SOEC and an F-T reactor, as shown in Fig. 1. In the SOEC anode, CH₄ and H₂O are supplied to anode with a ratio of 1:1.5 to avoid methane coking. CO₂ and H₂O are supplied to the cathode, where they are electrolyzed to generate syngas. Syngas generated from the SOEC section is collected for F-T reactor, where hydrocarbons are generated through the synthesis process.

2D numerical models are developed to simulate the characteristics of the system, the model kinetics for both the CH₄-assisted SOEC [21] and the F-T reactor [22] are validated by using prior published work. In accordance with the experimental work, the tubular SOEC adopted in the model has a length of 7 cm, an inner diameter of 0.3 cm and an outer diameter of 0.5 cm. It uses Ni-YSZ as anode support layer, Ni-ScSZ as anode active layer, ScSZ as electrolyte and Ni-ScSZ as cathode. The tubular F-T reactor has a length of 30 cm and an outer diameter of 1 cm. It uses Fe-based catalyst for the improvement of synthesis reaction rates. The material properties for the SOEC can be found in Table 1.

For model simplification and easier calculation, the following assumptions are adopted:

1. The triple phase boundaries are uniformly distributed in the porous electrodes as the ionic and electronic conducting materials are well mixed in the electrode preparing.
2. The electronic and ionic conducting phases are continuous and homogeneous in the porous electrodes as the electronic and ionic conducting materials are well mixed in the electrode preparing.
3. All the gases are considered as ideal gases because the effects of intermolecular forces and molecules sizes are less significant at high operating temperature.
4. Temperature distribution is uniform in the reactors due to the small size.

2.1. Sub-model of CH₄-assisted SOEC for CO₂ and H₂O co-electrolysis

As shown in Fig. 1, the gas mixture of H₂O and CO₂ flows into the cathode channel, while the gas mixture of CH₄ and H₂O flows into the anode channel. In the cathode, both H₂O and CO₂ are reduced to generate H₂ and CO as shown in Eq. (1) and Eq. (2), respectively.



In the anode, the methane steam reforming (MSR) reaction happens to generate H₂ and CO, which are then electrochemically oxidized by the O²⁻ ions transported from the cathode. The MSR reaction and electrochemical oxidations of H₂ and CO are listed as shown in Eqs. (3)–(5).



Due to the existence of H₂O and CO, water gas shift reaction

(WGS) occurs in both anode and cathode as shown in Eq. (6).



In operation, the required voltage applied to SOEC can be calculated by Eq. (7) as:

$$V = E + \eta_{\text{act}} + \eta_{\text{ohmic}} \quad (7)$$

where E is the equilibrium potential related with thermodynamics; η_{act} is the activation overpotentials reflecting the electrochemical activities and η_{ohmic} is the ohmic overpotential which can be calculated by the Ohmic law.

The calculation of equilibrium potential is based on oxygen partial pressure [23] and calculated as:

$$E = \frac{RT}{nF} \ln \left(\frac{\sum P_{\text{O}_2, \text{ca}}^L}{\sum P_{\text{O}_2, \text{an}}^L} \right) \quad (8)$$

where R is the universal gas constant (8.3145 J mol⁻¹ K⁻¹), T is temperature (K), F is the Faraday constant (96485 C mol⁻¹), n is the number of electrodes transferred per electrochemical reaction, $P_{\text{O}_2, \text{ca}}^L$ and $P_{\text{O}_2, \text{an}}^L$ are oxygen partial pressures in the cathode and anode, respectively.

For the pairs of H₂O/H₂ and CO₂/CO, their oxygen partial pressures can be expressed by:

$$P_{\text{O}_2, (\text{H}_2\text{O}/\text{H}_2)}^L = \left(\frac{P_{\text{H}_2\text{O}}^L}{P_{\text{H}_2}^L} \cdot e^{-\frac{\Delta G_{\text{H}_2\text{O}/\text{H}_2}}{RT}} \right)^2, \quad \text{and} \quad (9)$$

$$P_{\text{O}_2, (\text{CO}_2/\text{CO})}^L = \left(\frac{P_{\text{CO}_2}^L}{P_{\text{CO}}^L} \cdot e^{-\frac{\Delta G_{\text{CO}_2/\text{CO}}}{RT}} \right)^2, \quad (10)$$

where $P_{\text{H}_2\text{O}}^L$, $P_{\text{H}_2}^L$, $P_{\text{CO}_2}^L$ and P_{CO}^L are local partial pressures of H₂O, H₂, CO₂ and CO, respectively. $\Delta G_{\text{H}_2\text{O}/\text{H}_2}$ and $\Delta G_{\text{CO}_2/\text{CO}}$ are the Gibbs free energy change in the H₂ and CO oxidation reactions, respectively.

The activation overpotential is calculated by the Butler-Volmer equation as:

$$i = i_0 \left\{ \exp \left(\frac{\alpha n F \eta_{\text{act}}}{RT} \right) - \exp \left(\frac{-(1-\alpha) n F \eta_{\text{act}}}{RT} \right) \right\} \quad (11)$$

where i_0 is the exchange current density and α is the electronic transfer coefficient. For H₂O electrolysis, the exchange current density can be further expressed as:

$$i_0 = \beta \frac{P_{\text{H}_2\text{O}}^L}{P_{\text{ref}}} \frac{P_{\text{H}_2}^L}{P_{\text{ref}}} \exp \left(-\frac{E_a}{RT} \right) \quad (12)$$

where β is the activity factor and E_a is the activation energy. For CO₂ electrolysis, its exchange current density is 0.45 times of H₂O electrolysis [24]. All the kinetics for above reactions can be found in Table 2.

2.2. Sub-model of F-T reactor

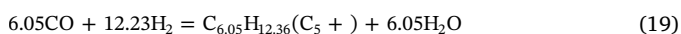
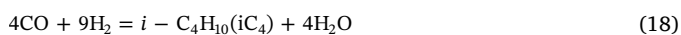
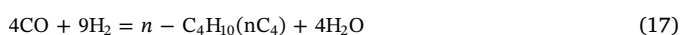
The F-T reactor uses Fe-HZSM5 as catalyst and works at 573 K and 2 MPa for syngas synthesis. The reactions in the F-T process are shown in Eqs. (13)–(20).

Table 1
Material properties.

Parameters	Value or expression	Unit
σ_{ScSZ}	$69,200 \times e^{-\frac{9681}{T}}$	S m ⁻¹
σ_{YSZ}	$33,400 \times e^{-\frac{10300}{T}}$	S m ⁻¹
σ_{Ni}	$4.2 \times 10^6 - 1065.3T$	S m ⁻¹
ϵ	0.36	
τ	3	
S _{TPB}	2.14×10^5	m ⁻¹

Table 2
Reaction kinetic parameters in SOEC section.

Parameters	Value or expression	Unit
β	3.3×10^8	A m^{-2}
E_a	1.2×10^5	J mol^{-1}
$\alpha_{\text{H}_2\text{O}}$	0.65	
α_{CO_2}	0.65	
R_{MSR} [27]	$k_{\text{rf}}(P_{\text{CH}_4}P_{\text{H}_2\text{O}} - \frac{P_{\text{H}_2}^3P_{\text{CO}}}{K_{\text{pr}}})$	$\text{mol m}^{-3} \text{s}^{-1}$
k_{rf}	$2395 \exp(\frac{-231266}{RT})$	$\text{mol m}^{-3} \text{Pa}^{-2} \text{s}^{-1}$
K_{pr}	$1.0267 \times 10^{10} \exp(-0.2513Z^4 + 0.3665Z^3 + 0.5810Z^2 - 27.134Z + 3.277)$	
R_{WGSR} [28]	$k_{\text{sf}}(P_{\text{H}_2\text{O}}P_{\text{CO}} - \frac{P_{\text{H}_2}P_{\text{CO}_2}}{K_{\text{ps}}})$	$\text{mol m}^{-3} \text{s}^{-1}$
k_{sf}	$0.0171 \exp(\frac{-103191}{RT})$	$\text{mol m}^{-3} \text{Pa}^{-2} \text{s}^{-1}$
K_{ps}	$\exp(-0.2935Z^3 + 0.6351Z^2 + 4.1788Z + 0.3169)$	
Z	$\frac{1000}{T} - 1$	



The reaction kinetics for above reactions can be expressed as shown in Eq. (21) [22].

$$R_i = 0.278k_i \exp(-\frac{E_i}{RT}) P_{\text{CO}}^m P_{\text{H}_2}^n \tag{21}$$

Related kinetics for reactions (13) to (20) are list in Table 3.

2.3. CFD Sub-model

For both the SOEC and the F-T reactor, the mass transport of gas species is calculated by extended Fick's law as shown in Eq. (22).

$$N_i = -\frac{1}{RT} \left(\frac{B_0 y_i P}{\mu} \nabla P - D_i^{\text{eff}} \nabla (y_i P) \right) \quad (i = 1, \dots, n) \tag{22}$$

Here B_0 is the material permeability, μ is the gas viscosity, y_i and D_i^{eff} are the mole fraction and effective diffusion coefficient of component i , respectively. D_i^{eff} can be further determined by

$$D_i^{\text{eff}} = \frac{\varepsilon}{\tau} \left(\frac{1}{D_{\text{im}}^{\text{eff}}} + \frac{1}{D_{\text{ik}}^{\text{eff}}} \right)^{-1} \tag{23}$$

where ε is the porosity, τ is the tortuosity factor, $D_{\text{im}}^{\text{eff}}$ is the molecular diffusion coefficient and $D_{\text{ik}}^{\text{eff}}$ is the Knudsen diffusion coefficient [25].

The mass conservation can be described by

$$\nabla \cdot (-D_i^{\text{eff}} \nabla c_i) = r_i \tag{24}$$

where c_i is the gas molar concentration and r_i is the mass source term of the gaseous species.

Navier-Stokes equation with Darcy's term is adopted to calculate the momentum transport in both the SOEC and F-T reactor as shown in Eq. (25).

$$\rho \frac{\partial \mathbf{u}}{\partial t} + \rho \mathbf{u} \nabla \cdot \mathbf{u} = -\nabla p + \nabla \cdot \left[\mu (\nabla \mathbf{u} + (\nabla \mathbf{u})^T) - \frac{2}{3} \mu \nabla \mathbf{u} \right] - \frac{\varepsilon \mu \mathbf{u}}{k} \tag{25}$$

Here ρ is the gas density and \mathbf{u} is the velocity vector.

2.4. Boundary conditions and model solution

Electric potentials are specified at the outer surface of two electrodes with the cell ends electrical insulated. Inlet gas flow rate and mole fraction of the species are given at inlets of the SOEC. The ratio of H_2 to CO for F-T reactor inlet is consistent with the ratio of H_2 to CO of SOEC cathode outlet. The numerical models are solved at given parameters using commercial software COMSOL MULTIPHYSICS® version 5.2.

3. Results and discussions

3.1. Model validation

In the SOEC sub-model, the same material and geometry are adopted in accordance with the experiments conducted by Luo et al. [24]. The kinetic parameters of the SOEC are validated by comparing the current-voltage characteristic of simulation results and experimental data with good agreement as shown in Fig. 2. In the subsequent parametric studies, the same cell structure and tuning parameters are used. The detailed operating conditions for model validation are given in Table 4.

In the Fisher-Tropsch sub-model, the same catalyst, operating temperature and pressure are used in accordance with the experiments. According to the testing and simulation results reported by Rahimpour et al. [22], the well validated power law kinetic model is adopted.

For above models, proper mesh densities are adopted with mesh independence validations conducted as shown in Fig. 2c and Fig. 2d.

3.2. Parametric studies

As shown in Fig. 3, CO and H_2 are generated in the SOEC and their mole fractions increase continuously from the inlet to the outlet. While in the F-T reactor, CO and H_2 are consumed and their mole fractions are

Table 3
Reaction kinetic parameters for F-T reactor.

Reaction number	m	n	k	E
13	-1.0889	1.5662	1.43×10^5	83423.9
14	0.7622	0.0728	5.16×10^1	65018.0
15	-0.5645	1.3155	2.47×10^1	49782.0
16	0.4051	0.6635	4.63×10^{-1}	34855.5
17	0.4728	1.1389	4.74×10^{-3}	27728.9
18	0.8204	0.5026	8.32×10^{-3}	25730.1
19	0.5850	0.5982	2.32×10^{-2}	23564.3
20	0.5742	0.7100	4.11×10^2	58826.3

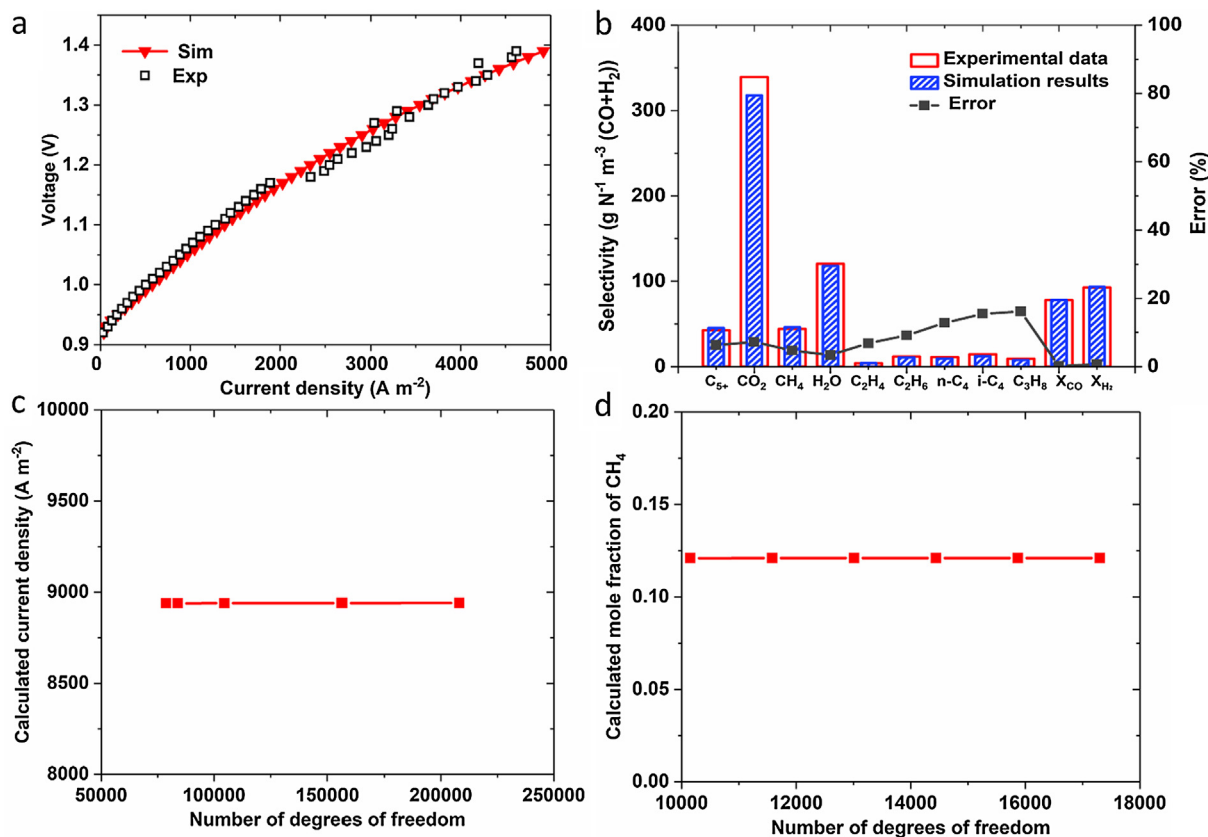


Fig. 2. Model validation for the (a) sub-model of CH₄-assisted SOEC for CO₂ and H₂O co-electrolysis, (b) sub-model of Fischer-Tropsch synthesis.

Table 4
Operation parameters for model validation.

Parameter	Value	Unit
Anode gas flow rate	150	SCCM
Cathode gas flow rate	350	SCCM
Anode gas composition	Air	
Cathode gas composition	CO ₂ (28.6%) + H ₂ O(28.6%) + H ₂ (14.3%) + N ₂ (28.5%)	
Temperature	1073	K

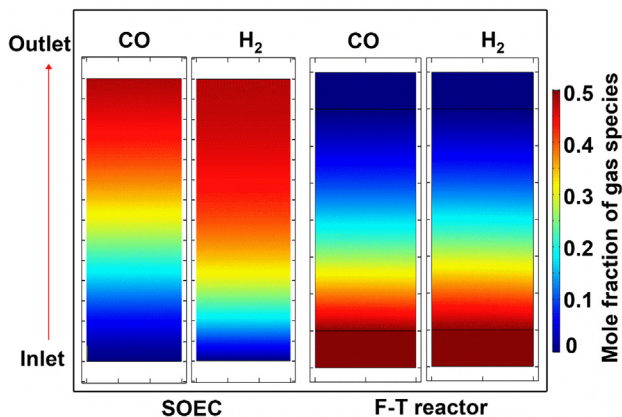


Fig. 3. Gas species (CO & H₂) distribution in the SOEC and Fischer-Tropsch reactor.

decreasing continuously from the inlet to the outlet. As syngas is the key intermediate in this hybrid system, the power consumption for generating syngas and hydrocarbons generated from syngas are detailed studied in the following parametric studies. Both cathode inlet

Table 5
Operating parameters for the study of inlet H₂O/CO₂ ratio.

Parameters	Value or expression	Unit
Anode inlet gas component	CH ₄ (40%) + H ₂ O (60%)	
Cathode inlet gas component	CO ₂ (10–90%) + H ₂ O	
Anode inlet gas flow rate	100	SCCM
Cathode inlet gas flow rate	100	SCCM
Input voltage	0.7	V
Operating temperature	1073	K

Table 6
Operating parameters for the study of applied voltage.

Parameters	Value or expression	Unit
Anode inlet gas component	CH ₄ (40%) + H ₂ O (60%)	
Cathode inlet gas component	CO ₂ (50%) + H ₂ O (50%)	
Anode inlet gas flow rate	100	SCCM
Cathode inlet gas flow rate	100	SCCM
Input voltage	0.1–0.7	V
Operating temperature	1073	K

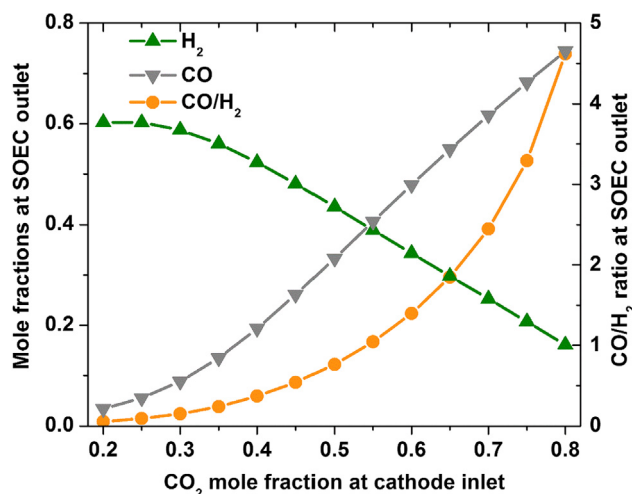


Fig. 4. Effects of CO₂ mole fraction at cathode inlet on H₂ and CO mole fractions at SOEC outlet.

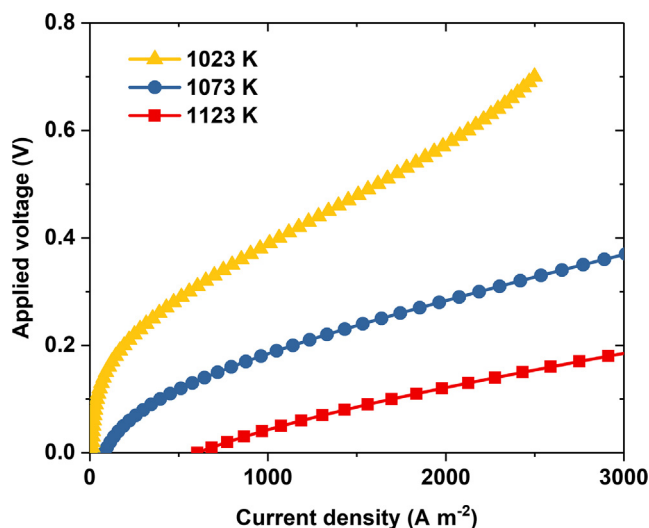


Fig. 7. Effects of operating temperature on the electrolysis power consumption.

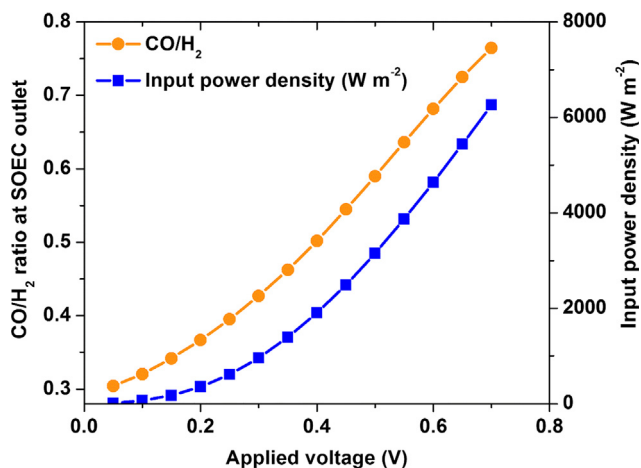


Fig. 5. Effects of applied voltage on CO/H₂ ratio of generated syngas and power consumption rate.

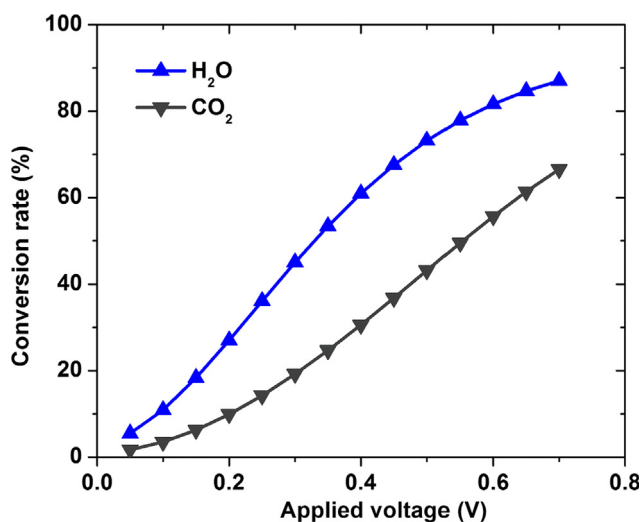


Fig. 6. Effects of applied voltage on H₂O and CO₂ conversion rate at SOEC section.

gas species and applied voltage are studies for the understanding and optimization of operating parameters. The detailed operating parameters are listed in Table 5 and Table 6.

3.2.1. Effects on the syngas mole fractions and power consumption rate

As the intermediate product, syngas is generated from SOEC and consumed in the F-T reactor. It has been proved by previous studies [26] that the CO/H₂ ratio has great effects on the methane selectivity and chain growth probability. Besides, the power consumption should also be considered for the optimization of economic efficiency. Therefore, it is important to study the factors that affects the generation of syngas as well as the power consumption rate in the production of syngas.

As shown in Fig. 4, the mole fractions of H₂ and CO at the SOEC cathode outlet are significantly affected by the CO₂ mole fraction at the inlet. With the increase of inlet CO₂ mole fraction, the mole fraction of produced CO rises quickly while the mole fraction of H₂ declines continuously. The CO/H₂ ratio is thus significantly improved with the increase of inlet CO₂ mole fraction, where the ratio is only 0.056 when CO₂ mole fraction at inlet is 0.2 while boosts to 4.6 when the CO₂ mole fraction at inlet increases to 0.8. This 80-times increase proves that it is effective to control the CO/H₂ ratio at SOEC outlet by adjusting the inlet CO₂/H₂O mole ratio.

The CO/H₂ ratio is also affected by the applied voltage as shown in Fig. 5. In accordance with previous reports [21], the SOEC can work at a lower applied voltage with fuel assistance. In addition, a lower CO/H₂ ratio at SOEC outlet can be obtained with the decrease of applied voltage. For comparison, the CO/H₂ ratio at SOEC outlet is 0.76 at 0.7 V applied voltage while decreases to less than half (0.3) at 0.05 V applied voltage. Moreover, the input power density is significantly declined with the decrease of applied voltage, where the power density is 6258 W m⁻² at 0.7 V while decreases to 17 W m⁻² at 0.05 V. However, the conversion rate of both H₂O and CO₂ also drop quickly with the decrease of applied voltage as shown in Fig. 6. At 0.7 V applied voltage, the conversion rate of H₂O and CO₂ are 87% and 67%, respectively. While at 0.05 V applied voltage, the conversion rate of H₂O and CO₂ drop to 5.5% and 1.7%, which is too low for practical application. The power consumption of electrolysis is also affected by the operating temperature of SOEC as shown in Fig. 7. At 2000 A m⁻² operating current density, 0.57 V input voltage is required when the SOEC is working at 1023 K operating temperature. When the operating temperature increases to 1123 K, only 0.12 V input voltage is required, which means about 80% of power consumption can be saved in this case.

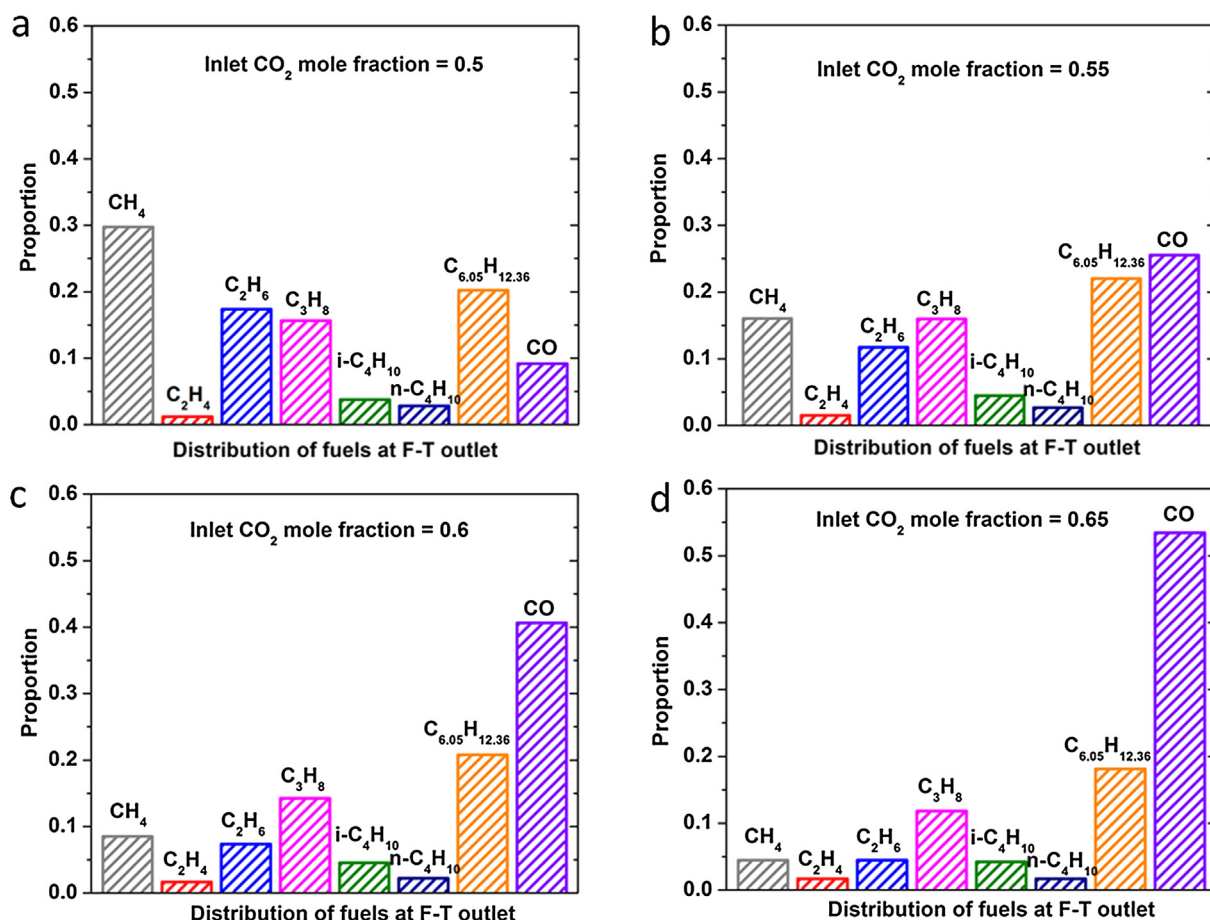


Fig. 8. Effects of CO₂ mole fractions at cathode inlet on the distribution of fuels at F-T outlet.

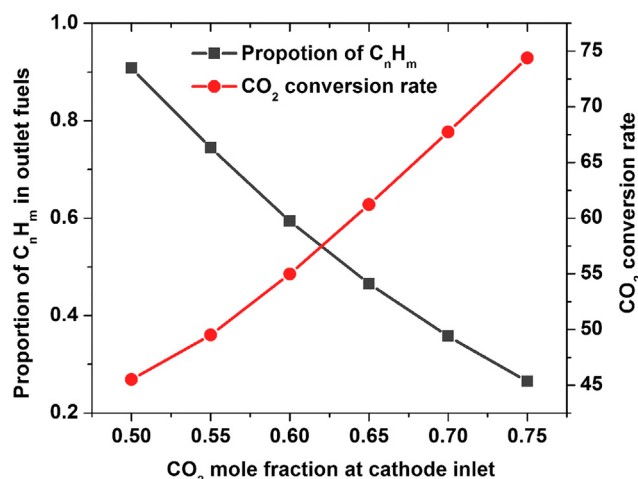


Fig. 9. Effects of CO₂ mole fractions at cathode inlet on proportion of hydrocarbons in the outlet fuels and CO₂ conversion rate.

3.2.2. Effects on the distribution of fuels at F-T outlet

Considering the conversion from CO₂ to carbon-contained fuels, the proportions of C atoms among the carbon-contained fuels (including CH₄ (C₁), C₂H₄, C₂H₆ (C₂), C₃H₈ (C₃), i-C₄H₁₀, n-C₄H₁₀, C_{6.05}H_{12.36} (C₅₊) and CO) are calculated. The proportion of C atoms in each fuel is calculated as $P = \frac{C_i}{C_{total}}$, where C_i is the amount of C atoms contained in one specific fuel and C_{total} is the amount of C atoms contained in all the fuels.

As shown in Fig. 8, when the CO₂ mole fraction at inlet is 0.5, the largest part of C atoms (30%) is contained in CH₄ among all the fuels,

while only 20% C atoms are contained in C₅₊, and there are still 9% CO not fully used. With the increase of inlet CO₂ mole fraction, the C atoms contained in CH₄ continuously decreases, where there are only 16%, 9% and even 4% C atoms contained in CH₄ at 0.55, 0.6 and 0.65 inlet CO₂ mole fractions, respectively. On the other hand, the C atoms contained in CO increases quickly with the increase of CO₂ mole fractions at inlet, where 26%, 41% and 53% C atoms are contained in CO at 0.55, 0.6 and 0.65 inlet CO₂ mole fractions, respectively. The proportion of C atoms contained in C₅₊ is relatively stable with the change of inlet CO₂ mole fraction, which only varies between 22% and 18% at given operating parameters. As CH₄ can be recycled to be utilized in the SOEC section and a high CO conversion rate is preferred, a lower inlet CO₂ mole fraction is thus suggested through above analysis.

The proportion of C atoms contained in hydrocarbons (C_nH_m) and CO₂ conversion rate is also given as shown in Fig. 9. Although the proportion of C_nH_m continuously decreases (from 90% to 26%) with the increase of inlet CO₂ mole fraction, the significant increase of CO₂ conversion rate (from 46% to 74%) is still attractive in the utilization of CO₂.

4. Conclusions

In this paper, the first 2D model combining a CH₄-assisted solid oxide co-electrolysis and Fischer-Tropsch synthesis system for CO₂ utilization and hydrocarbon generation is developed. The kinetics of the model are validated by using previous studies. CO₂ and H₂O are used as the feedstock to produce low-carbon fuel through the F-T reactor. Through parametric studies, the effects of CO₂ (H₂O) mole fraction on the production of syngas is studied. It is found that it is effective to control the CO/H₂ ratio of the syngas by adjusting the CO₂/H₂O ratio at

the SOEC inlet. Besides, the applied voltage is also varied for the parametric study, where the applied voltage and operating temperature are found to significantly affect the power consumption rate as well as the CO₂ and H₂O conversion rate. Finally, the distribution of carbon-contained fuels generated by the F-T reactor is studied. The proportions of C atoms among different fuels are compared, where it is found that the inlet CO₂ (H₂O) mole fraction significantly affects the proportion of fuels, particularly CH₄ and CO in the F-T outlet. In general, the mole fractions of hydrocarbons from C₁ to C₅₊ generated by the F-T reactor can be controlled by adjusting the inlet H₂O/CO₂ ratio in the electrolysis process. This study builds a solid foundation for the understanding and optimization of a combined fuel-assisted SOEC and F-T reactor system. Based on this preliminary work, a higher-level model is still needed, which can give a detailed analysis on the integration of this low-carbon fuel generation technology with other energy conversion-storage hubs.

Acknowledgements

The research is supported by the UK Engineering and Physical Sciences Research Council (EPSRC) through grants EP/K021796/1 and EP/N009924/1.

References

- [1] Kregel D, Samsun RC, Peters R, Stolten D. The separation of CO₂ from ambient air – A techno-economic assessment. *Appl Energy* 2018;218:361–81. <https://doi.org/10.1016/j.apenergy.2018.02.144>.
- [2] Laguna-Bercero MA. Recent advances in high temperature electrolysis using solid oxide fuel cells: A review. *J Power Sources* 2012;203:4–16. <https://doi.org/10.1016/j.jpowsour.2011.12.019>.
- [3] Kim-Lohsoontorn P, Bae J. Electrochemical performance of solid oxide electrolysis cell electrodes under high-temperature coelectrolysis of steam and carbon dioxide. *J Power Sources* 2011;196:7161–8. <https://doi.org/10.1016/j.jpowsour.2010.09.018>.
- [4] Ni M, Leung MKH, Leung DYC. Technological development of hydrogen production by solid oxide electrolyzer cell (SOEC). *Int J Hydrogen Energy* 2008;33:2337–54. <https://doi.org/10.1016/j.ijhydene.2008.02.048>.
- [5] Li W, Wang H, Shi Y, Cai N. Performance and methane production characteristics of H₂O–CO₂ co-electrolysis in solid oxide electrolysis cells. *Int J Hydrogen Energy* 2013;38:11104–9. <https://doi.org/10.1016/j.ijhydene.2013.01.008>.
- [6] Zhang H, Wang J, Su S, Chen J. Electrochemical performance characteristics and optimum design strategies of a solid oxide electrolysis cell system for carbon dioxide reduction. *Int J Hydrogen Energy* 2013;38:9609–18. <https://doi.org/10.1016/j.ijhydene.2013.05.155>.
- [7] Zheng H, Tian Y, Zhang L, Chi B, Pu J, Jian L. La_{0.8}Sr_{0.2}Co_{0.8}Ni_{0.2}O_{3-δ} impregnated oxygen electrode for H₂O/CO₂ co-electrolysis in solid oxide electrolysis cells. *J Power Sources* 2018;383:93–101. <https://doi.org/10.1016/j.jpowsour.2018.02.041>.
- [8] Xu H, Chen B, Tan P, Zhang H, Yuan J, Liu J, et al. Performance improvement of a direct carbon solid oxide fuel cell system by combining with a Stirling cycle. *Energy* 2017;140:979–87. <https://doi.org/10.1016/j.energy.2017.09.036>.
- [9] Xu H, Chen B, Tan P, Zhang H, Yuan J, Irvine JTS, et al. Performance improvement of a direct carbon solid oxide fuel cell through integrating an Otto heat engine. *Energy Convers Manage* 2018;165:761–70. <https://doi.org/10.1016/j.enconman.2018.04.008>.
- [10] Xu H, Chen B, Tan P, Cai W, Wu Y, Zhang H, et al. A feasible way to handle the heat management of direct carbon solid oxide fuel cells. *Appl Energy* 2018;226:881–90. <https://doi.org/10.1016/j.apenergy.2018.06.039>.
- [11] Tao G, Butler B, Virkar A. Hydrogen and power by fuel-assisted electrolysis using solid oxide fuel cells. *ECS Trans* 2011;35:2929–39. <https://doi.org/10.1149/1.3570292>.
- [12] Luo Y, Shi Y, Li W, Ni M, Cai N. Elementary reaction modeling and experimental characterization of solid oxide fuel-assisted steam electrolysis cells. *Int J Hydrogen Energy* 2014;39:10359–73. <https://doi.org/10.1016/j.ijhydene.2014.05.018>.
- [13] Xu H, Chen B, Ni M. Modeling of direct carbon-assisted Solid Oxide Electrolysis Cell (SOEC) for syngas production at two different electrodes. *J Electrochem Soc* 2016;163:F3029–35. <https://doi.org/10.1149/2.0041611jes>.
- [14] Gaudillere C, Navarrete L, Serra JM. Syngas production at intermediate temperature through H₂O and CO₂ electrolysis with a Cu-based solid oxide electrolyzer cell. *Int J Hydrogen Energy* 2014;39:3047–54. <https://doi.org/10.1016/j.ijhydene.2013.12.045>.
- [15] Chen B, Xu H, Ni M. Modelling of SOEC-FT reactor: Pressure effects on methanation process. *Appl Energy* 2017;185:814–24. <https://doi.org/10.1016/j.apenergy.2016.10.095>.
- [16] Chen B, Xu H, Chen L, Li Y, Xia C, Ni M. Modelling of one-step methanation process combining SOECs and Fischer-Tropsch-like reactor. *J Electrochem Soc* 2016;163:F3001–8. <https://doi.org/10.1149/2.0011611jes>.
- [17] Cao P, Adegbite S, Zhao H, Lester E, Wu T. Tuning dry reforming of methane for F-T syntheses: A thermodynamic approach. *Appl Energy* 2018;227:190–7. <https://doi.org/10.1016/j.apenergy.2017.08.007>.
- [18] Qin S, Chang S, Yao Q. Modeling, thermodynamic and techno-economic analysis of coal-to-liquids process with different entrained flow coal gasifiers. *Appl Energy* 2018;229:413–32. <https://doi.org/10.1016/j.apenergy.2018.07.030>.
- [19] Becker WL, Braun RJ, Penev M, Melaina M. Production of Fischer-Tropsch liquid fuels from high temperature solid oxide co-electrolysis units. *Energy* 2012;47:99–115. <https://doi.org/10.1016/j.energy.2012.08.047>.
- [20] Stempien JP, Ni M, Sun Q, Chan SH. Thermodynamic analysis of combined Solid Oxide Electrolyzer and Fischer-Tropsch processes. *Energy* 2015;81:682–90. <https://doi.org/10.1016/j.energy.2015.01.013>.
- [21] Xu H, Chen B, Irvine J, Ni M. Modeling of CH₄-assisted SOEC for H₂O/CO₂ co-electrolysis. *Int J Hydrogen Energy* 2016;41:21839–49. <https://doi.org/10.1016/j.ijhydene.2016.10.026>.
- [22] Rahimpour MR, Elekaei H. A comparative study of combination of Fischer-Tropsch synthesis reactors with hydrogen-permeable membrane in GTL technology. *Fuel Process Technol* 2009;90:747–61. <https://doi.org/10.1016/j.fuproc.2009.02.011>.
- [23] Stempien JP, Liu Q, Ni M, Sun Q, Chan SH. Physical principles for the calculation of equilibrium potential for co-electrolysis of steam and carbon dioxide in a Solid Oxide Electrolyzer Cell (SOEC). *Electrochim Acta* 2014;147:490–7. <https://doi.org/10.1016/j.electacta.2014.09.144>.
- [24] Luo Y, Shi Y, Li W, Cai N. Comprehensive modeling of tubular solid oxide electrolysis cell for co-electrolysis of steam and carbon dioxide. *Energy* 2014;70:420–34. <https://doi.org/10.1016/j.energy.2014.04.019>.
- [25] Suwanwarangkul R, Croiset E, Fowler MW, Douglas PL, Entchev E, Douglas MA. Performance comparison of Fick's, dusty-gas and Stefan-Maxwell models to predict the concentration overpotential of a SOFC anode. *J Power Sources* 2003;122:9–18. [https://doi.org/10.1016/S0378-7753\(02\)00724-3](https://doi.org/10.1016/S0378-7753(02)00724-3).
- [26] Malek Abbaslou RM, Soltan Mohammadzadeh JS, Dalai AK. Review on Fischer-Tropsch synthesis in supercritical media. *Fuel Process Technol* 2009;90:849–56. <https://doi.org/10.1016/j.fuproc.2009.03.018>.
- [27] Ni M. 2D heat and mass transfer modeling of methane steam reforming for hydrogen production in a compact reformer. *Energy Convers Manage* 2013;65:155–63. <https://doi.org/10.1016/j.enconman.2012.07.017>.
- [28] Ni M. An electrochemical model for syngas production by co-electrolysis of H₂O and CO₂. *J Power Sources* 2012;202:209–16. <https://doi.org/10.1016/j.jpowsour.2011.11.080>.